Atmospheric Environment 330 (2024) 120561

Contents lists available at ScienceDirect

Atmospheric Environment

journal homepage: www.elsevier.com/locate/atmosenv

Nighttime ozone excess days and the associated meteorological conditions in the North China Plain from 2015 to 2022

Jia Xue, Hong Liao *, Jiandong Li

Jiangsu Key Laboratory of Atmospheric Environment Monitoring and Pollution Control, Jiangsu Collaborative Innovation Center of Atmospheric Environment and Equipment Technology, School of Environmental Science and Engineering, Nanjing University of Information Science & Technology, Nanjing, 210044, China

HIGHLIGHTS

- We examined the nighttime ozone excess days (NOEDs) in NCP during 2015–2022.
- The frequency of NOEDs in 91.23% of cities in NCP had an upward trend over 2015–2022.
- Two types of regional NOEDs were identified, which had different weather types.

GRAPHICAL ABSTRACT

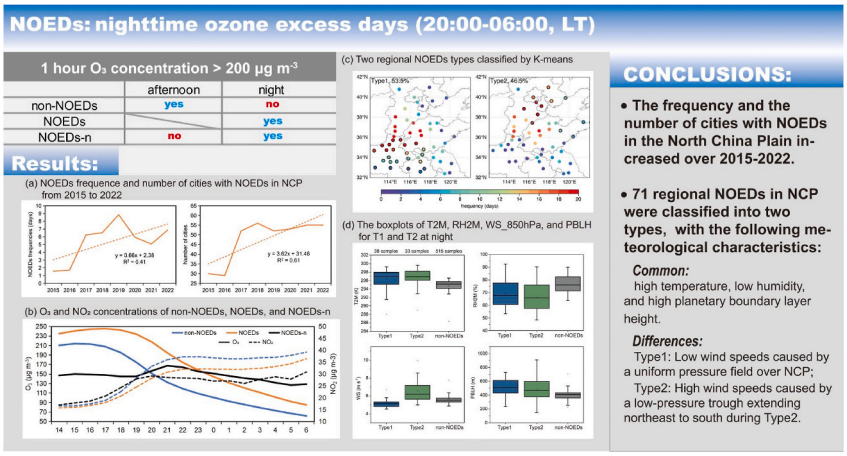

ARTICLE INFO

Keywords:
Nighttime ozone excess
Meteorological conditions
Atmospheric circulation pattern

ABSTRACT

We examined the spatial and temporal variations of nighttime ozone (O_3) excess days (NOEDs) in the North China Plain (NCP) during 2015–2022 by using the observed O_3 concentrations from the China National Environmental Monitoring Center network. The NOEDs were defined as those with any 1-h average O_3 concentration at night (20:00 to 06:00 local time) exceeding 200 μg m^{-3}. The observations showed that the annual frequencies of NOEDs averaged over the 57 cities in the NCP were 1.56, 1.72, 6.23, 6.53, 8.84, 5.93, 5.07, and 6.86 days in 2015, 2016, 2017, 2018, 2019, 2020, 2021, and 2022, respectively, with a linear increasing trend of 0.66 d y^{-1}. Using the K-means clustering method, two typical regional NOEDs types in the NCP were identified. Type1 had the highest frequencies of NOEDs in the southwest of NCP, while Type2 had the highest frequencies in the central NCP region. These two types contributed to 53.5% and 46.5% of the regional NOEDs in NCP, respectively. Compared with the regional non-NOEDs (with nighttime O_3 did not exceed but daytime O_3 exceeded O_3 air quality standard), both Type1 and Type2 NOEDs generally had higher temperature, lower relative humidity, and higher planetary boundary height in both afternoon and night, favoring the production and accumulation of O_3 in the afternoon as well as the persistent high O_3 at night. Corresponding weather patterns were also identified.

* Corresponding author.
E-mail address: hongliao@nuist.edu.cn (H. Liao).

https://doi.org/10.1016/j.atmosenv.2024.120561
Received 13 February 2024; Received in revised form 17 April 2024; Accepted 5 May 2024
Available online 6 May 2024

These results have important implications for emission control strategies during NOEDs. Emission control measures can be applied once the dominant circulation patterns have been predicted.

1. Introduction

Surface ozone (O_3) is a major air pollutant that has detrimental effects on public health and crop yields (Lefohn et al., 2018; Ma et al., 2016; Nuvolone et al., 2018; Turner et al., 2016; Wang et al., 2007; Yue et al., 2017). O_3 is produced by photochemical reactions of volatile organic compounds (VOCs) and nitrogen oxides (NO_x) (Chu et al., 2020; Gao et al., 2017; Jacob, 2000; Jena et al., 2015). Daily O_3 concentrations typically peak in the afternoon when sunlight is the strongest and gradually decrease after sunset due to chemical destruction and dry deposition (Seinfeld and Pandis, 2016; Zhang et al., 2004). However, China has experienced frequent occurrences of nighttime ozone excess days (NOEDs), defined as those with any 1-h average O_3 concentration at night (20:00 to 06:00 of local time (LT)) exceeding 200 μg m^{-3}. Understanding the spatial and temporal variations of NOEDs is crucial for effective air quality planning in China.

High concentrations of nighttime O_3 influence both meteorology and atmospheric chemistry. A substantial amount of nocturnal O_3 enhances the absorption of longwave radiation from the ground, leading to local heating and thereby affecting the accuracy of temperature predictions (Kulkarni et al., 2013). Nocturnal O_3 can oxidize nitrogen dioxide (NO_2), resulting in the production of nitrogen pentoxide (N_2O_5), which further autoionizes to form nitrate (NO_3^-) and nitrite ions (NO_2^+). These compounds then react with hydrogen chloride (HCl) to produce nitrochloride ($ClNO_2$) (Raff et al., 2009). $ClNO_2$ is light-sensitive and can generate Cl radicals, playing a crucial role in rapidly initiating O_3 generation in the troposphere during the early morning (Ravishankara, 2009). Moreover, high concentrations of nighttime O_3 can provide a high initial concentration for photochemical reactions on the following day, leading to a subsequent increase in O_3 concentration during the day (Jia et al., 2015).

Previous studies generally concluded that nighttime O_3 enhancements were caused by meteorological conditions since nighttime emissions were about the same throughout a month or a season. San José et al. (2005) used the OPANA Air Quality Modeling System to simulate an nighttime high O_3 episode in Madrid, and reported that the episode was caused by winds to Madrid which changed direction by 180° and brought back O_3 generated the day before. Hu et al. (2013) analyzed an nighttime O_3 enhancement event in Beltsville, Maryland, U.S. on August 9–10, 2010, by using observed meteorological parameters from balloons, O_3 concentrations from O_3 sondes, and the WRF-Chem model. They found that the low-level jet induced strong turbulence to transport O_3-rich air from the residual layer to the surface. Bao et al. (2017) found that the transport of O_3 from the upwind area to Dalian exacerbated local O_3 pollution at night of 2015 by back-trajectory analyses. Previous studies, However, were generally focused on nocturnal ozone enhancement events at one or a few sites and were limited to timescales of days or months.

Few studies have examined the temporal and spatial variations of nocturnal O_3 in China. Wang et al. (2022a) examined the O_3 trends in the city of Rizhao (an industrialized city on the east coast of China) and found that the growth rate of nighttime O_3 (2.6% y^{-1}) was higher than that of daytime O_3 (0.8% y^{-1}) over 2014–2020. They also found that the ratio of the 2014–2020 change in nighttime mean O_3 concentration to that in daily mean O_3 was 68.5%. He et al. (2022) defined nocturnal ozone enhancement as an O_3 increase of more than 5 ppbv h^{-1} in 1 of any 2 adjacent hours from 20:00 to 06:00 LT, and investigated the nocturnal ozone enhancement events in China from 2014 to 2020 by using the hourly observations of surface O_3, NO_2, and carbon monoxide (CO) from the China National Environmental Monitoring Center (CNEMC) network. They found that the frequency of the nocturnal ozone enhancement events was high in the warm seasons in industrialized city clusters (especially in the North China Plain (NCP)). However, to our knowledge, no previous studies have examined the spatial and temporal variations of NOEDs.

Previous studies attempted to identify the weather patterns that determined the high levels of air pollutants. Zhang et al. (2016) used the Kirchhofer classification technique to classify the circulation patterns from 1980 to 2014 in NCP into five categories and found that the high air pollution indices were related to the stable weather conditions in this region. Liao et al. (2023) obtained four distinct ozone diurnal patterns in Beijing from 2013 to 2020 by applying K-means clustering. They found that the abnormal nocturnal boundary layer (NBL) meteorological conditions in Beijing were conducive to the high concentration of O_3 at night. Therefore, in this work, we examine weather conditions conducive to NOEDs in the NCP, which helps for understanding the formation mechanism of NOEDs events.

The scientific goals of this study are as follows: 1) to examine the frequency, intensity, spatial distribution, and temporal variation of NOEDs over China from 2015 to 2022 by using the observed hourly O_3 concentrations from CNEMC; 2) to identify the typical patterns of regional NOEDs (defined as days in which more than 20% of cities in NCP experienced NOEDs) in NCP by using the K-Means clustering method; 3) to identify the key meteorological parameters and weather patterns that led to the formation of NOEDs.

Section 2 presents the data and methods used in this study, including the descriptions of the studied area, observational data, and the K-means clustering method. Section 3 presents the spatial distribution and temporal variation of NOEDs over NCP, the major types of regional NOEDs, and the key meteorological parameters and weather patterns for the formation of NOEDs.

2. Data and methods

2.1. Studied area

According to the observed annual frequency of NOEDs in China from 2015 to 2022 (Fig. S1), NOEDs occurred at 997 sites during these years, and NCP (112°-122°E, 32°-42°N) is the region with the highest frequency. Therefore, we chose NCP as the studied area in this work. NCP is one of the most polluted regions in China, with Taihang Mountain located in the western NCP and the Bohai and Yellow Seas located to the east. There are 57 cities in NCP as shown in Fig. 1, including Beijing and Tianjin, 11 cities in Hebei province, 16 cities in Shandong province, 15 cities in Henan province, 6 cities in Anhui province, and 7 cities in Jiangsu province.

2.2. Observed concentrations of air pollutants

Hourly O_3, NO_2 and $PM_{2.5}$ concentrations over China from 2015 to 2022 were obtained from CNEMC network. The datasets have been widely used in previous studies (He et al., 2022; Li et al., 2021; Liu and Wang, 2020). The concentrations of O_3 and NO_2 were reported by the CNEMC under standard conditions of 273 K and 1013 hPa until August 31, 2018, and of 298 K and 1013 hPa afterward (https://www.mee.gov.cn/xxgk2018/xxgk/xxgk01/201808/t20180815_629602.html). To maintain the consistency of the observed concentration, we re-scaled post-August 2018 O_3 and NO_2 concentrations to the pre-August 2018 standard conditions. All downloaded concentrations were selected following these steps: 1) days without valid data during night (20:00–06:00 LT) were excluded, and 2) sites with less than 90% valid data since January 2015 were also removed. In this study, the

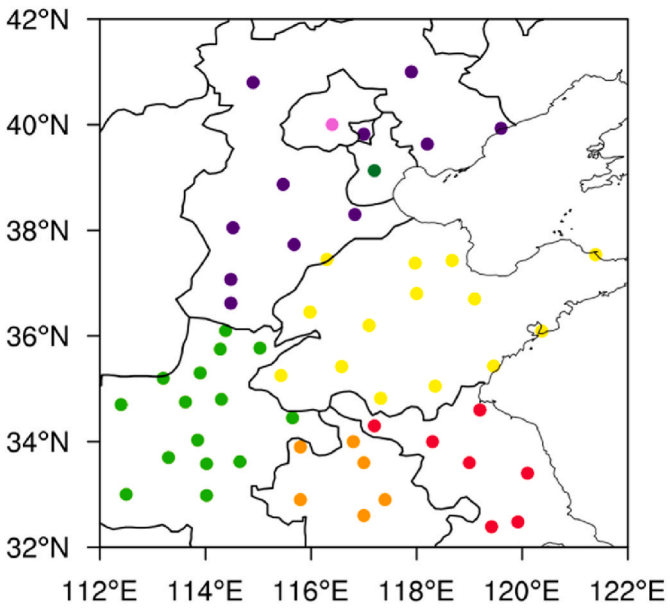

Fig. 1. Spatial distribution of cities with observed concentrations of pollutants in the North China Plain. The colors represent 7 provinces or municipalities in the NCP. The dots with purple, green, yellow, orange, red, pink, and dark green represent Hebei, Henan, Shandong, Anhui, Jiangsu, Beijing, and Tianjin, respectively.

concentration of a city was calculated as the average of concentrations of all sites within that city.

The 1-h average concentration limit of O_3 is 200 μg m^{-3} following the National Ambient Air Quality Standard of China (GB3095-2012). We define NOEDs as the days with any 1-h average concentration of O_3 at night (20:00–06:00 LT) above 200 μg m^{-3}. A total of 2661 NOEDs occurred in the NCP from 2015 to 2022, in which 2548 (95.75%) events were accompanied by hourly exceedance of O_3 Air Quality Standard in the afternoon whereas 113 samples (4.25%) did not exceed the standard in the afternoon. Regional NOEDs are defined as days in which more than 20% of cities in NCP experienced NOEDs. The O_3 standards in China remained consistent from 2015 to 2022, therefore, we used the same criteria for regional NOEDs that occurred from 2015 to 2022, which can display the long-term trend of NOEDs. This standard of screening regional pollution events based on the number of polluting cities within the region has been widely applied in previous research (Wei et al., 2021; Zong et al., 2021). As a result, 71 days (samples) were found to have regional NOEDs in NCP during 2015–2022. The distributions of NOEDs in NCP for these 71 selected regional NOEDs events were shown in Fig. S2. The cities with NOEDs were mostly adjacent and the characteristics of geographical locations will be classified by K-means clustering algorithm as described in Section 2.4.

2.3. Meteorological data

The meteorological parameters were taken from the MERRA2 reanalyzed dataset of NASA's Global Modeling and Assimilation Office (https://gmao.gsfc.nasa.gov/reanalysis/MERRA-2/). The temporal resolution is 1 h and the spatial resolution is 0.5° latitude × 0.625° longitude. The meteorological parameters we used include temperature (T), relative humidity (RH), geopotential height (H), wind (U/V) speed and direction, and planetary boundary layer height (PBLH).

2.4. Classification of NOEDs by K-means clustering algorithm

To identify the predominant NOEDs types that influence nighttime air quality over the NCP, the K-means algorithm was used to cluster NOEDs events that occurred during 2015–2022. This method has been widely used in studies of extreme events (Chang and Zhan, 2017; Salimi et al., 2014). 57 cities and 71 regional NOEDs days were permuted to a 0–1 two-dimensional array (city vs. time) for clustering. For each city in NCP, daily sample values were set to 1 when NOEDs occurred, and 0 for non-NOEDs days. Then 71 regional NOEDs were assigned to a specific number of clusters by the K-means clustering algorithm.

To optimize the classification, a set of classification configurations with numbers 2–7 was considered, with the two-type classification identified as being optimal by Monte Carlo simulation (more categories did not result in more meaningful classification types, as shown in Figs. S3–7). The further details of the K-means algorithm and Monte Carlo tests were explained in the Supplementary data.

3. Results

3.1. Spatiotemporal variations of NOEDs in NCP

Fig. 2a shows the spatial distributions of frequencies of NOEDs in NCP for years 2015–2022. In 2015 and 2016, NOEDs occurred in about 30 cities, in which only 2 cities (Beijing and Chengde) had frequencies of NOEDs that exceeded 10 days y^{-1}. From 2017 to 2019, the NOEDs frequencies increased significantly, with 14 cities in 2017, 12 cities in 2018, and 21 cities in 2019 had NOEDs of exceeding 10 days y^{-1}. The frequencies reached the highest value of 22 days in 4 cities (Tianjin, Shijiazhuang, Handan, and Liaocheng) in 2019. In 2020 and 2021, the frequencies of NOEDs decreased slightly relative to 2019, but NOEDs were still serious in terms of both the frequency and the coverage.

The annual NOEDs frequencies averaged over the 57 cities in NCP were 1.56, 1.72, 6.23, 6.53, 8.84, 5.93, 5.07, and 6.86 days in 2015, 2016, 2017, 2018, 2019, 2020, 2021, and 2022, respectively, with a linear increasing trend of 0.66 d y^{-1} (Fig. 2b). In addition, the number of cities with NOEDs in NCP showed a linear trend of 3.62 cities y^{-1} over 2015–2022, with 91.23% (52/57 cities) of cities had an upward trend. The number reached the maximum of 57 cities in 2018 and maintained a relatively high level since then (more than 50 cities every year after 2018) (Fig. 2c).

Fig. 3a shows the monthly mean nighttime (20:00–06:00 LT) concentrations of O_3 and NOEDs frequencies averaged over NCP from 2015 to 2022. The frequencies of NOEDs were generally higher as nighttime O_3 concentrations were higher, with a positive correlation coefficient of 0.7 between NOEDs frequencies and nighttime O_3 concentrations. The nighttime O_3 concentration and NOEDs frequency reached their highest values of 107.99 μg m^{-3} and 5.19 days, respectively, in June of 2022. Over 2015–2022, NOEDs occurred generally during April–September, with 60.3% of NOEDs occurring in June. The variation in NO_2 concentration was opposite to that of O_3, usually low in summer (June, July, and August) and had its lowest value in July (except for in August 2019 and in February 2019) (Fig. 3b).

To examine daily variations of NOEDs, we classified O_3 polluted days into three kinds: non-NOEDs, NOEDs, and NOEDs-n. Non-NOEDs were those (15299 samples during 2015–2022) with nighttime O_3 did not exceed but daytime O_3 exceeded the O_3 air quality standard, NOEDs were those (2661 samples) with nighttime O_3 exceeded the O_3 air quality standard (including daytime exceeded and daytime not exceeded the standard), and NOEDs-n were those (113 samples) with nighttime O_3 exceeded but daytime O_3 not exceeded the standard. O_3 formation occurs as a result of the photolysis of NO_2. One would expect that the concentration of O_3 is the highest and that of NO_x is low in the afternoon when solar radiation is the strongest. After sunset, nitric oxide (NO) reacts rapidly with O_3, resulting in an increase in NO_2 and a decrease in O_3 concentration.

Fig. 4a shows the composited daily variations of O_3 and NO_2 for 15299 non-NOEDs samples in NCP during 2015–2022. The average concentration of O_3 reached its highest (213.64 μg m^{-3}) at 15:00 (LT), and then gradually decreased. The average O_3 concentrations in the

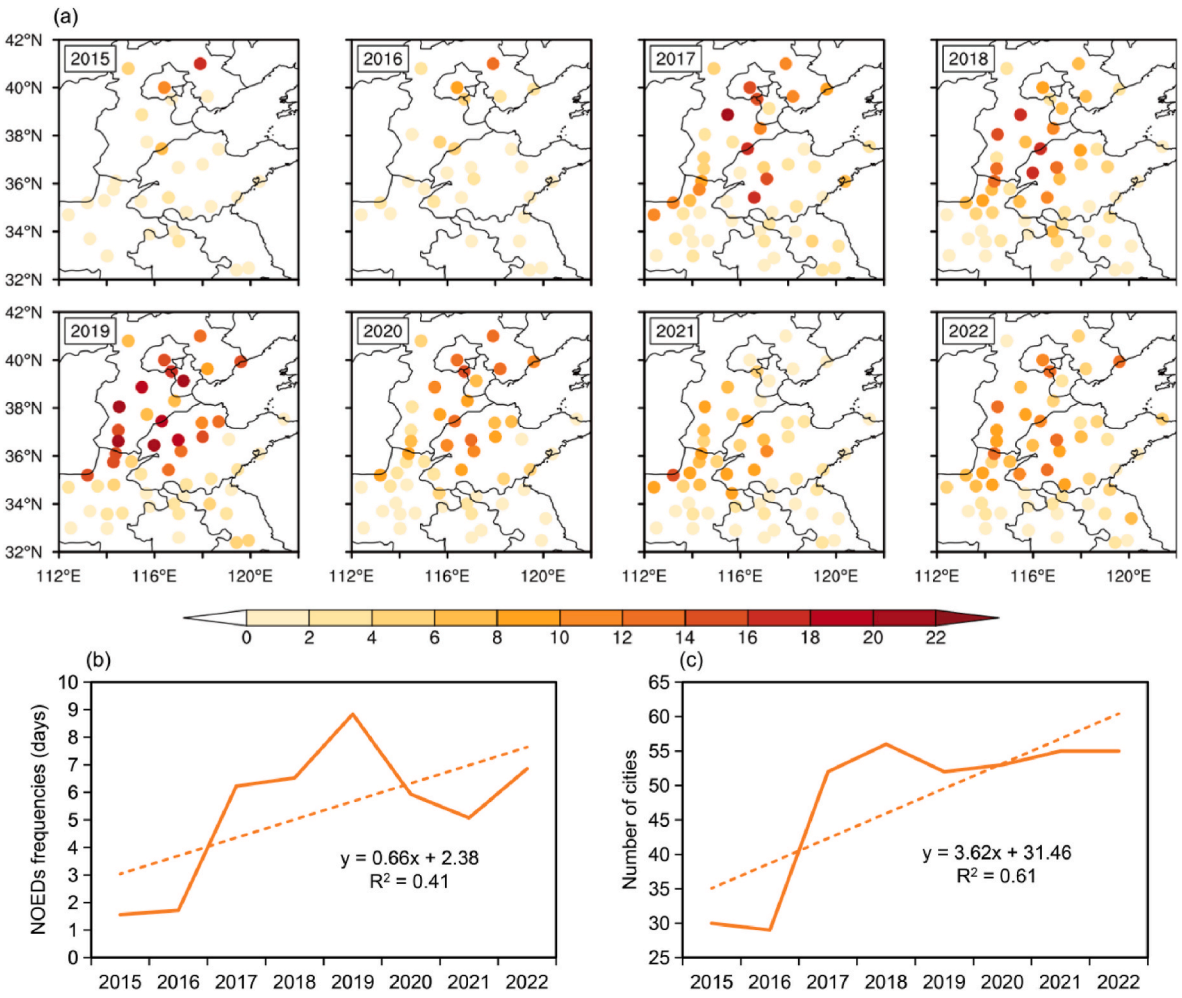

Fig. 2. (a) Spatial distributions of observed NOEDs (days yr $^{-1}$) in the NCP from 2015 to 2022, (b) Annual variations of NOEDs frequencies averaged over 57 cities in NCP, and (c) Number of cities with NOEDs in NCP from 2015 to 2022.

afternoon (14:00–19:00 LT) and nighttime (20:00–06:00 LT) were 202.23 and 97.43 μg m^{-3}, respectively. NO reacts quickly with O_3 to generate NO_2 after sunset, and the rate of increase of NO_2 reached its highest at 19:00. The average NO_2 concentration in the nighttime was 36.70 μg m^{-3}.

For 2661 NOEDs samples in NCP during 2015–2022 (Fig. 4b), concentrations of O_3 peaked at 17:00 (245.07 μg m^{-3}) and the averaged O_3 concentrations in the afternoon and nighttime were 240.00 μg m^{-3} and 139.26 μg m^{-3}, respectively, which were higher than the values of non-NOEDs samples. However, the mean NO_2 concentration in the nighttime was 32.25 μg m^{-3}, which was lower than that of non-NOEDs samples. For 113 NOEDs-n samples in NCP for years 2015–2022 (Fig. 4c), the highest concentration of O_3 (165.89 μg m^{-3}) occurred at 21:00, and the averaged O_3 concentration in the afternoon (nighttime) was lower by 94.08 μg m^{-3} (higher by 5.55 μg m^{-3}) compared to NOEDs. The growth rate of daily NO_2 concentration was relatively high around 18:00. The average NO_2 concentration in the nighttime was 28.10 μg m^{-3} and reached its highest at 20:00.

We also examined the hourly frequencies and locations for regional NOEDs as defined in Section 2.2. 71 samples were screened out for all months during 2015–2022. Fig. 5 shows the frequencies of O_3 concentrations exceeding 200 μg m^{-3} at night (20:00–08:00 LT) in cities in NCP considering 71 regional NOEDs. It is interesting that O_3 exceedances mainly occurred from 20:00 to 23:00, and the frequencies of occurrence gradually decreased with time. Unlike the photochemical reactions during the daytime, there is no light at night, so NO_2 cannot photolysis to produce O_3. However, NO will continue to deplete O_3, resulting in a continuous decrease in O_3 concentration at night. This also indicates that O_3 exceedances at night were closely related to high O_3 concentrations during the daytime.

3.2. Classification of regional NOEDs

To identify the typical regional NOEDs types in the NCP from 2015 to 2022, we built a two-dimensional array containing 57 cities and 71 sample days and then clustered the daily regional NOEDs records over the NCP by using the K-means clustering method as described in Section 2.4. Two typical regional NOEDs were identified; Type1 and Type2 were responsible for 53.5% (38 days) and 46.5% (33 days), respectively, of the 71 regional NOEDs in the NCP.

Fig. 6a presents the spatial distributions of the frequencies of Type1 NOEDs in 57 cities. The 23 cities (1 in Heibei, 3 in Shandong, 5 in Anhui, and 14 in Henan) exceeding the 95% significance level were located in the southwestern NCP. Because Taihang Mountain is located to the west of NCP and hence the atmospheric diffusion of the urban agglomeration in the southwestern NCP is unfavorable. The hourly variations of O_3, $PM_{2.5}$, and NO_2 concentrations averaged over the 23 cities show that concentrations of Type1 NOEDs generally had smaller standard deviations than those of Type2 NOEDs (Fig. 7), which were caused by the unfavorable weather conditions for diffusion as discussed in the next Section. The average concentrations of O_3, $PM_{2.5}$, and NO_2 in the afternoon (14:00–19:00 LT) (nighttime, 20:00–06:00 LT) were,

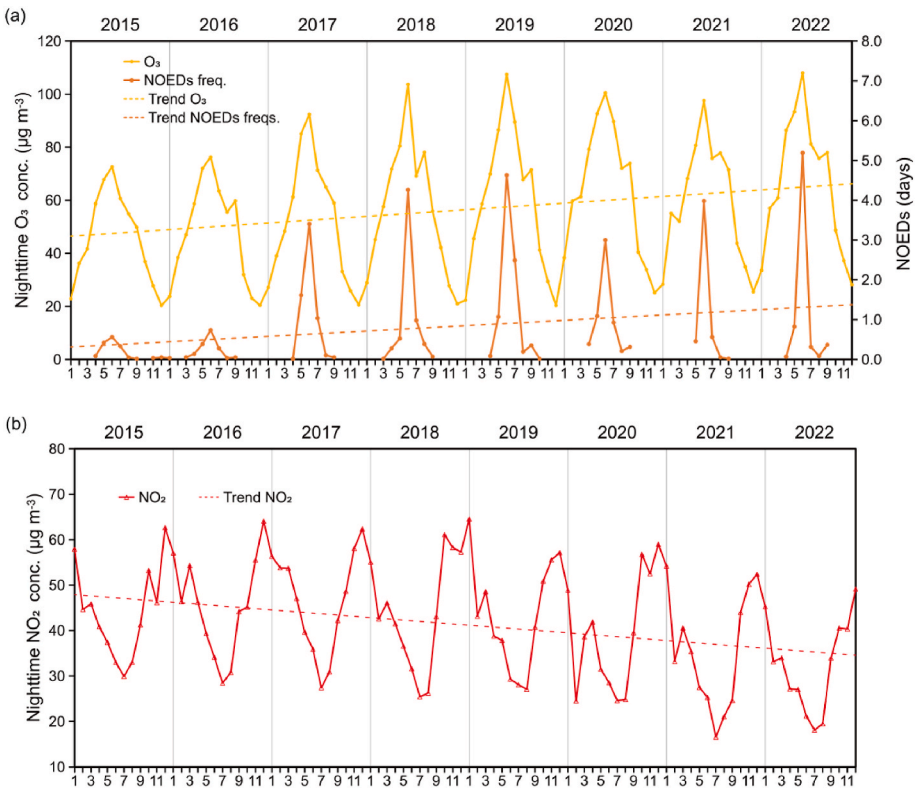

Fig. 3. (a) Monthly mean nighttime (20:00–06:00 LT) O_3 concentrations (μg m^{-3}) and monthly NOEDs frequencies (days) averaged over NCP over 2015–2022. (b) Monthly mean concentrations (μg m^{-3}) of nighttime NO_2 averaged over NCP over 2015–2022.

respectively, 223.4 (124.2) μg m^{-3}, 32.5 (38.8) μg m^{-3}, and 15.0 (28.9) μg m^{-3} for Type1 NOEDs (Fig. 7). Among the 38 samples of Type 1 regional NOEDs, the highest frequency occurred in June (84.2%), followed by July (13.2%) and May (2.6%) (Fig. S8).

The spatial distribution of the frequencies of Type2 NOEDs in 57 cities was different from Type1. The 12 cities (Beijing, Tianjin, 5 in Shandong, and 5 in Hebei) exceeding the 95% significance level were located in northern NCP (Fig. 6b). The hourly concentrations of O_3, $PM_{2.5}$, and NO_2 averaged over the 12 cities had large standard deviations, and the average concentrations of these three species in the afternoon (nighttime) were 239.68 (127.11) μg m^{-3}, 36.88 (44.14) μg m^{-3}, and 20.43 (32.94) μg m^{-3} (Fig. 7), respectively. Similar to Type1, Type2 had the highest frequencies in June (78.8%), followed by May (15.1%), and July (6.1%) (Fig. S8).

The areas with high O_3 concentrations during Type1 and Type2 were located in the southwestern and northern NCP, respectively, and the distributions of O_3 concentrations in the afternoon were about the same as those at night (Fig. S9). The spatial distributions of NO_2 were similar for Type1 and Type2, but Type2 had higher NO_2 concentrations in the central part of NCP (especially in the Beijing-Tianjin-Hebei region) and the eastern coast (Fig. S10).

3.3. Meteorological conditions for the occurrence of regional NOEDs

During NOEDs, nighttime O_3 concentrations were closely related to daytime O_3 concentrations (Section 3.1), and nighttime O_3 cannot be photochemically generated. Therefore, the continuous accumulation of high concentrations of O_3 from daytime to nighttime under favorable meteorological conditions is expected to be a key reason for high nighttime O_3 concentrations. Atmospheric temperature and relative humidity have been found to have dominant impacts on daytime O_3 concentrations (Gong and Liao, 2019). High atmospheric temperature is conducive to photochemical O_3 formation, and low humidity leads to slow chemical removal of O_3 (Wang et al., 2022b; Yu et al., 2019). Furthermore, high concentrations of O_3 are often accompanied by daytime high PBLH and low wind speed (Dong et al., 2020; Ren et al., 2021; Su et al., 2018). Therefore, we carry out composited analyses on afternoon and nighttime meteorological parameters for the two types of regional NOEDs in the NCP, including T at 2 m (T2M), RH at 2 m (RH2M), wind speed at 850 hPa (WS850), and PBLH (Fig. 8). These meteorological parameters in Fig. 8 were from the MERRA2 reanalyzed datasets. Because MERRA2 datasets are available every 1 h, we have selected meteorological fields of 13:30–18:30 to represent afternoon and 19:30–05:30 to represent nighttime.

For Type1, these meteorological parameters were averaged over 38 regional NOEDs samples. In both afternoon and night, temperatures were the highest in the southwestern NCP, consistent with the region with the highest frequencies of Type1 NOEDs. In this region, RH2M was the lowest in NCP and PBLH was relatively high from afternoon to night. In the afternoon (at nighttime), compared with the regional non-NOEDs (with nighttime O_3 did not exceed but daytime O_3 exceeded O_3 air quality standard, 515 samples), averaged Type1 NOEDs had higher T2M by 2.92 K (1.67 K), lower RH2M by 9.89% (7.26%), and higher PBLH by 384.85 m (109.88 m), and lower WS850 by 0.77 m s^{-1} (0.43 m s^{-1}) (Fig. 8). All these weather conditions contributed to the generation and accumulation of local O_3 in the afternoon. The low windspeed and its small deviation led to the persistent high O_3 concentrations and small deviations of O_3 concentrations at night.

Fig. 8 also shows the averages of meteorological parameters in the afternoon and nighttime for 33 samples of Type2 NOEDs. The area with high T2M, high PBLH and low RH2M was in the middle of NCP, which corresponded well with the high frequencies of Type2 NOEDs. In the afternoon (at nighttime), compared with the 515 regional non-NOEDs samples, averaged Type2 NOEDs had higher T2M by 3.31 K (2.08 K), lower RH2M by 11.65% (10.31%), and higher PBLH by 382.84 m (73.58 m), which were also conducive to the generation of local O_3. Different from Type1, strong southwesterlies prevailed in the NCP during days of Type2 NOEDs, and WS850 in the afternoon (at nighttime)

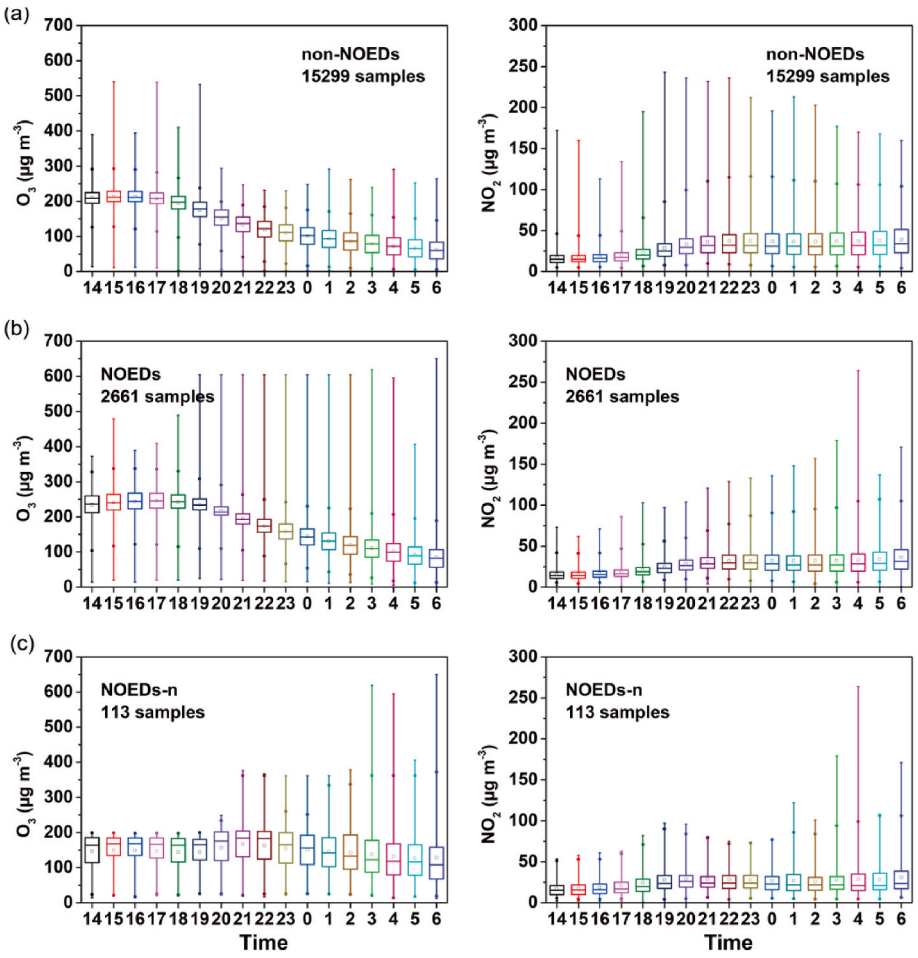

Fig. 4. Composited daily variations of concentrations (μg m^{-3}) of O_3 and NO_2 for (a) non-NOEDs (nighttime O_3 did not exceed but daytime O_3 exceeded O_3 air quality standard, 15299 samples), (b) NOEDs (nighttime O_3 exceeded O_3 air quality standard, with daytime O_3 either exceeded and not exceeded the standard, 2661 samples), (c) NOEDs-n (nighttime O_3 exceeded but daytime O_3 not exceeded the standard, 113 samples). The samples accounted for the 57 cities in NCP during 2015–2022. The upper and lower ends of the whisker indicate the maximum and minimum values, and the upper and lower ends of the box are the 75% and 25% percentiles. The horizontal line represents the mean value. The round dots show the 1% and 99% percentiles.

was higher by 0.66 m s^{-1} (0.94 m s^{-1}) relative to regional non-NOEDs. Large deviations in RH2M, WS850, and PBLH resulted in the large standard deviation of nighttime O_3 concentrations of Type2 NOEDs.

We also chose Zhengzhou, Shijiazhuang, Beijing, and Chengde (from the southwest to the northeast of NCP) as examples to analyze the hourly variation of O_3 concentrations from afternoon to night for Type1 and Type2 (Fig. S11). In Type1, the time of O_3 to peak in these four cities was relatively close (at 15:00 and 16:00). However, in Type2, there was a clear chronological order of the occurrence of O_3 peaks, from the southwest to the northeast of NCP with Zhengzhou (14:00), Shijiazhuang (16:00), Beijing and Chengde (17:00), indicating that the strong southwesterlies in Type2 caused the order of the occurrence of O_3 peaks in the downwind areas.

3.4. Dominant synoptic weather patterns for regional NOEDs in the NCP

To further understand the typical weather patterns beneficial for NOEDs in NCP, we conducted composited analyses of sea level pressure (SLP)/geopotential height (HGT) and winds for the surface layer and altitudes of 850 hPa and 500 hPa for Type1 and Type2 NOEDs at night (Fig. 9).

For Type1 NOEDs (38 regional Type1 NOEDs samples), a cold vortex was located over the northeastern China and the NCP was to the southwest of it at 500 hPa. At 850 hPa and the surface, NCP was located within a uniform pressure field between the Japanese offshore low pressure and the Mongolian low pressure, leading to a stagnant weather condition with low wind speed and slow air diffusion in the North China, which were favorable for the accumulation of O_3. In addition, at the surface, the easterlies caused by the weak high-pressure ridge brought relatively clean marine atmosphere to the eastern coastal areas of NCP, resulting in lower O_3 concentrations in Type1 than in Type2 (Fig. 7).

For Type2 (33 regional NOEDs days), at 500 hPa, a cold vortex over Japan restricted the westward extension of the Western Pacific Subtropical High, and the areas from Xinjiang to North China were controlled by the continental high-pressure ridge, resulting in high temperature and low humidity, which were favorable for the generation of O_3 and were consistent with Fig. 8. At 850 hPa, the weak anticyclonic to the south of NCP caused high-speed southerlies. This airflow passed through the urban agglomeration in the southwest of NCP and brought relatively polluted air to the central and northeastern NCP. In addition, the central NCP had more favorable meteorological conditions for O_3 generation with higher temperature and lower humidity compared to Type1 (Fig. 8), resulting in the formation of Type2 NOEDs in central NCP (Fig. 6). The large standard deviation in high-speed wind also led to a large standard deviation in O_3 concentrations (Fig. 7). The southerlies maintained the high levels of O_3 because of the transport of upwind pollutants.

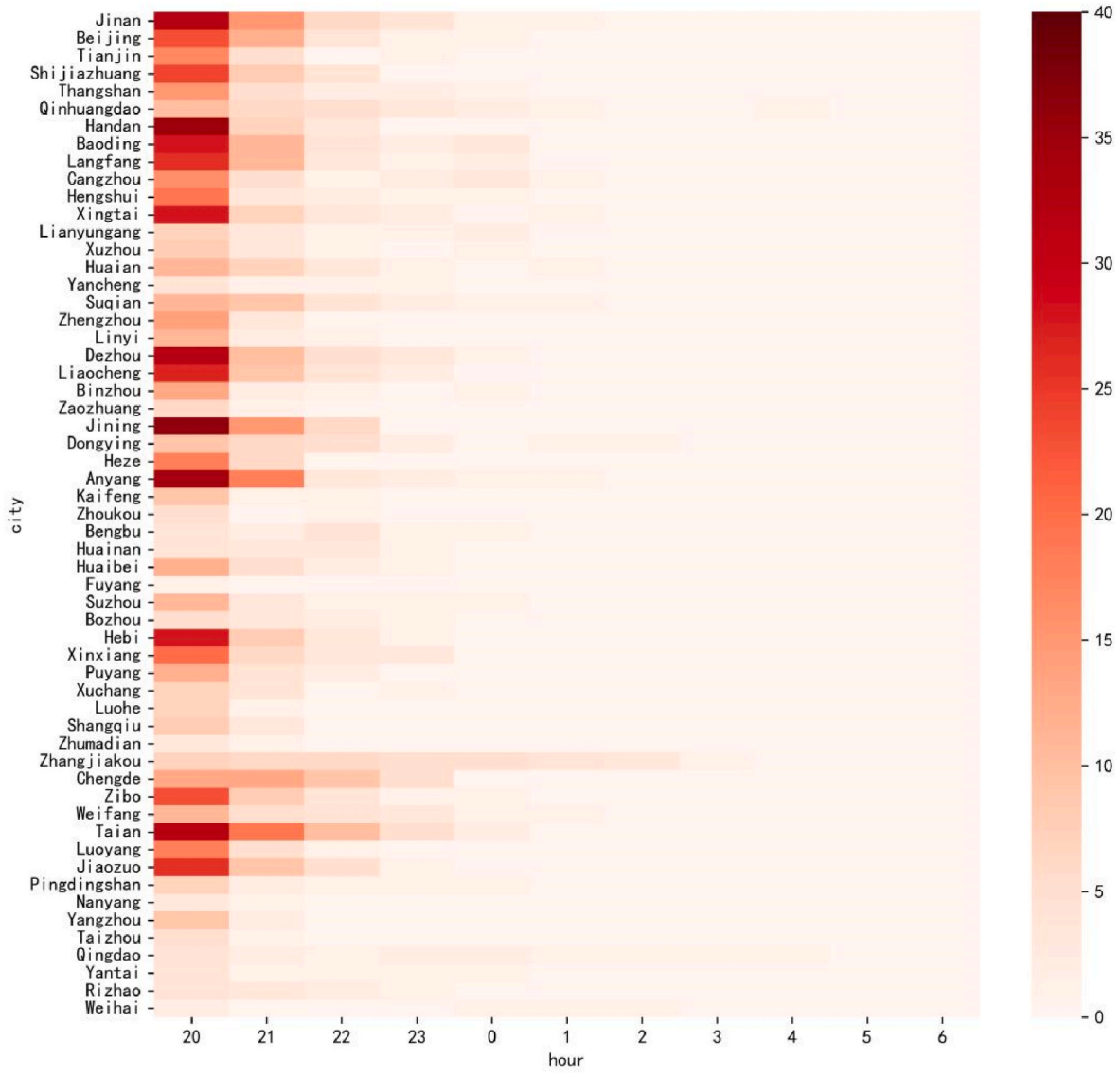

Fig. 5. Frequency (days) of O_3 exceeding 200 μg m^{-3} at night (20:00–08:00 LT) in 57 cities in the NCP considering 71 regional NOEDs.

4. Conclusions

In this study, we examined the spatial distribution and temporal variation of NOEDs (days with any 1-h average concentration of O_3 at night (20:00–06:00 LT) above 200 μg m^{-3}) over the NCP region by using the observed O_3 concentrations from 2015 to 2022. Considering all the 57 cities in NCP, a total of 2661 NOEDs occurred during 2015–2022, in which 2548 (95.75%) days were accompanied by hourly exceedance of O_3 Air Quality Standard in the afternoon whereas 113 samples (4.25%) did not exceed the standard in the afternoon. The annual NOEDs frequencies averaged over the 57 cities in NCP were 1.56, 1.72, 6.23, 6.53, 8.84, 5.93, 5.07, and 6.86 days in 2015, 2016, 2017, 2018, 2019, 2020, 2021, and 2022, respectively, with a linear increasing trend of 0.66 d y^{-1}. The number of cities with NOEDs in NCP showed a linear trend of 3.62 cities yr^{-1} over 2015–2022, with 91.23% (52/57 cities) of cities had an upward trend.

During 2015–2022, 71 days were found to have regional NOEDs (more than 20% of cities in NCP experienced NOEDs), with the highest number of frequencies seen in the months of May, June, and July. By using the K-means clustering method, two typical regional NOEDs types in the NCP were identified. Type1 had the highest frequencies of NOEDs in the southwestern NCP, while Type2 had the highest frequencies in the central NCP region. These two types contributed to 53.5% and 46.5% of the regional NOEDs in NCP, respectively.

Meteorological conditions for Type1 regional NOEDs were examined. Composited analyses showed that NCP was located within a uniform pressure field between the Japanese offshore low pressure and the Mongolian low pressure at 850 hPa and the surface, leading to a stagnant weather condition. In the afternoon (at nighttime), compared with the regional non-NOEDs (with nighttime O_3 did not exceed but daytime O_3 exceeded O_3 air quality standard, 515 samples), averaged Type1 NOEDs had higher T2M by 2.92 K (1.67 K), lower RH2M by 9.89% (7.26%), and higher PBLH by 384.85 m (109.88 m), and lower WS850 by 0.77 m s^{-1} (0.43 m s^{-1}). All these weather conditions contributed to the generation and accumulation of local O_3 in the afternoon as well as the persistent high O_3 concentrations at night.

Meteorological conditions for Type2 regional NOEDs were also identified. In the afternoon (at nighttime), compared with the 515 regional non-NOEDs samples, averaged Type2 NOEDs had higher T2M by 3.31 K (2.08 K), lower RH2M by 11.65% (10.31%), and higher PBLH by 382.84 m (73.58 m), which were also conducive to the generation of local O_3. Different from Type1, strong south-westerlies prevailed in the NCP during Type2 events, and WS850 in the afternoon (at nighttime) was higher by 0.66 m s^{-1} (0.94 m s^{-1}) relative to regional non-NOEDs.

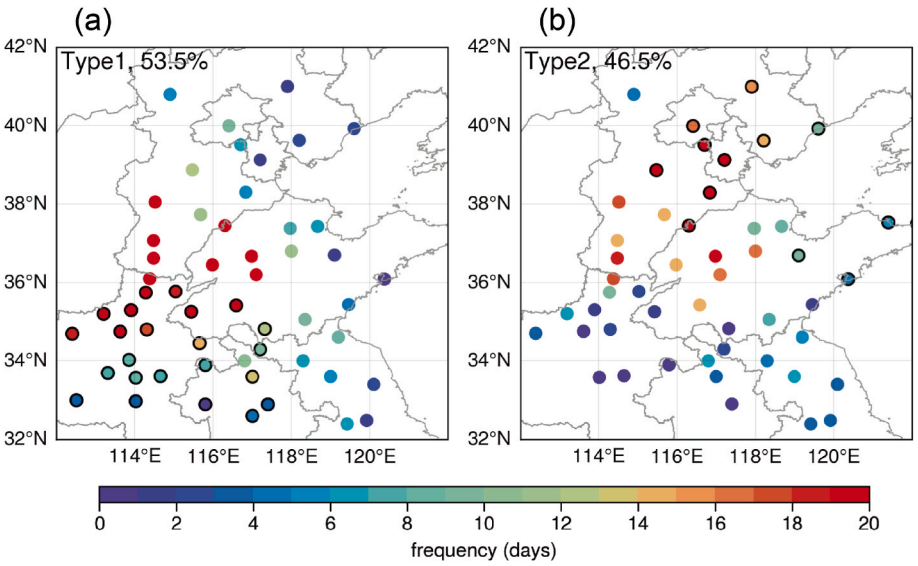

Fig. 6. Spatial distributions of the frequencies (days) of Type1 and Type2 NOEDs in 57 cities during 2015–2022 based on K-means clustering (k = 2). Dots with black circles indicate sites exceeding the 95% significance level (Monte Carlo test). There were 38 regional Type1 NOEDs and 33 regional Type2 NOEDs, which contributed to 53.5% and 46.5% of the regional NOEDs in NCP during the studied years, respectively.

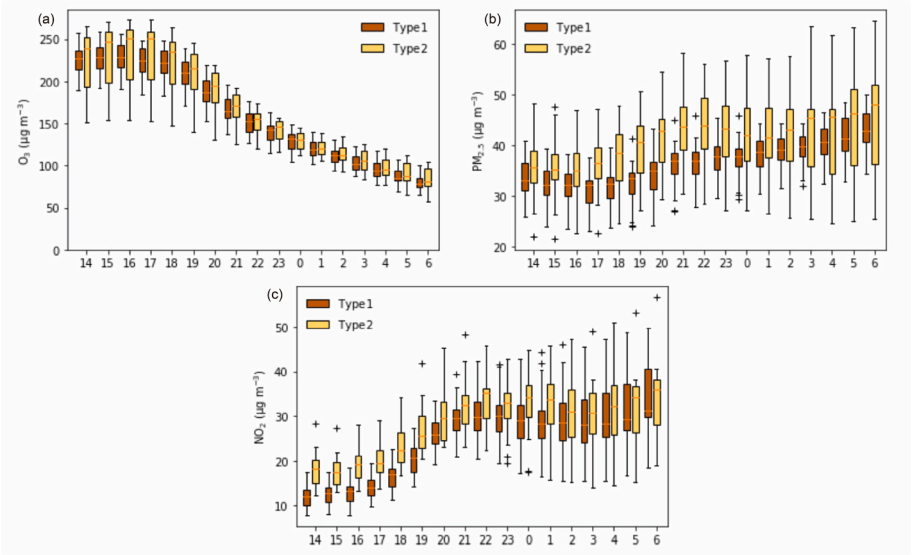

Fig. 7. The composited hourly mean concentrations (μg m^{-3}) of (a) O_3, (b) $PM_{2.5}$, and (c) NO_2 for cities with a significance level exceeding 95% for Type1 and Type2 NOEDs. The upper and lower ends of the whisker indicate the maximum and minimum values, and the upper and lower ends of the box are the 75% and 25% percentiles. The horizontal line represents the mean value. Plus sign indicates discrete values.

The weak anticyclonic to the south of NCP at 850 hPa caused high-speed southerlies, which passed through the urban agglomeration in the southwest of NCP and brought relatively polluted air to the central and northeastern NCP.

This study identified the increasing trends of NOEDs in NCP, which have important implications for emission control strategies for ozone pollution. Strengthening emission control measures is needed when circulation patterns of NOEDs are predicted, especially during severe O_3 pollution in summer.

Finally, it is important to note that, this study did not further discuss the contribution of interannual changes in precursor emissions to daytime and nighttime NOEDs, which will be further explored in subsequent work.

CRediT authorship contribution statement

Jia Xue: Writing – original draft, Software, Methodology, Data curation, Conceptualization. **Hong Liao:** Writing – review & editing, Supervision, Resources, Conceptualization. **Jiandong Li:** Resources.

Declaration of competing interest

The authors declare that they have no known competing financial interests or personal relationships that could have appeared to influence the work reported in this paper.

Data availability

Data will be made available on request.

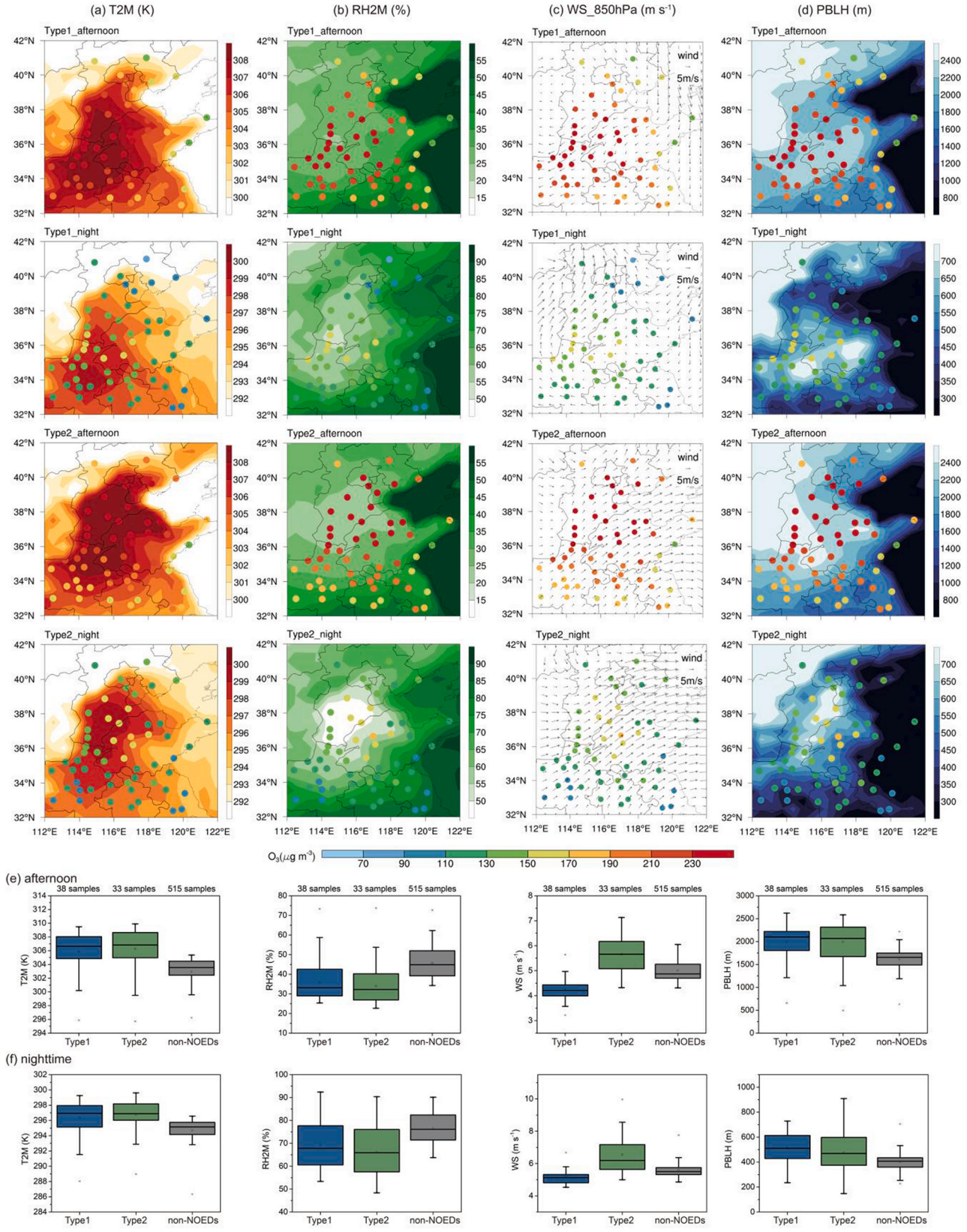

Fig. 8. (a)–(d) Composites of T2M (temperature at 2 m, K), RH2M (relative humidity, %), WS_850 hPa (wind speed at 850 hPa, m s^{-1}), and PBLH (planetary boundary layer height, m) relative to the surface O_3 concentrations (μg m^{-3}) in the NCP (57 cities). The overlying dots represent the averaged O_3 concentrations over the studied time periods at 57 cities in the NCP. (e)–(f) The boxplots of T2M, RH2M, WS at 850 hPa, and PBLH for Type1 regional NOEDs, Type2 regional NOEDs, and regional non-NOEDs in 57 cities in NCP for afternoons and nights. The upper and lower ends of the whisker indicate the maximum and minimum values, and the upper and lower ends of the box show the 75% and 25% percentiles. The horizontal line represents the mean value.

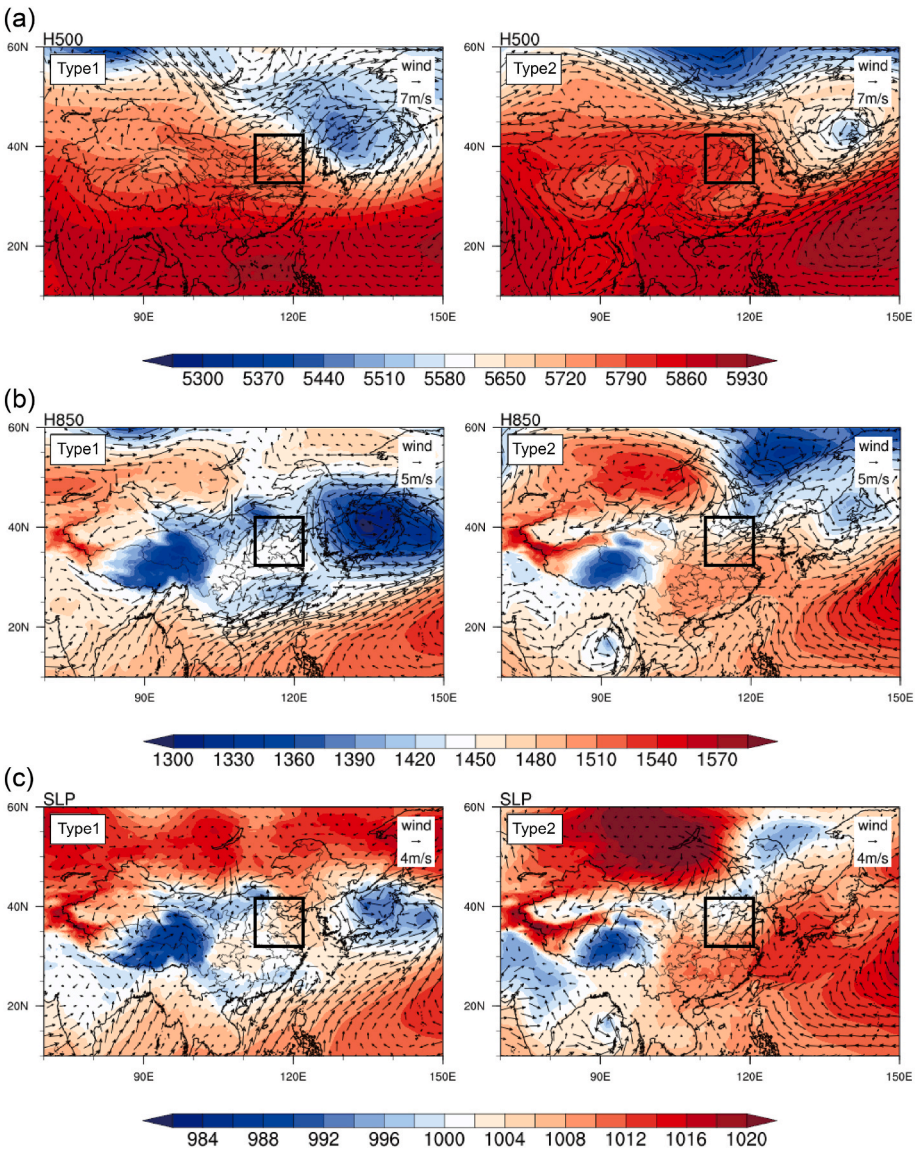

Fig. 9. Composited weather patterns for 2 typical regional NOEDs types in the NCP. (a) geopotential height (m) and wind field (m s^{-1}) at 500 hPa, (b) geopotential height (m) and wind field (m s^{-1}) at 850 hPa, and (c) Sea level pressure (hPa) and wind field (m s^{-1}) at 10 m.

Acknowledgments

This work was supported by the National Natural Science Foundation of China under grants 42293320 and 42021004.

Appendix A. Supplementary data

Supplementary data to this article can be found online at https://doi.org/10.1016/j.atmosenv.2024.120561.

References

Bao, Y., Xu, J., Zhang, M., Tang, W., Meng, F., 2017. The characteristics of ozone pollution and causes of A typical ozone pollution episode in dalian. Environ. Monit. China 33 (4), 167–178. https://doi.org/10.19316/j.issn.1002-6002.2017.04.21.

Chang, W., Zhan, J., 2017. The association of weather patterns with haze episodes: recognition by $PM_{2.5}$ oriented circulation classification applied in Xiamen, Southeastern China. Atmos. Res. 197, 425–436. https://doi.org/10.1016/j.atmosres.2017.07.024.

Chu, B., Ma, Q., Liu, J., Ma, J., Zhang, P., Chen, T., Feng, Q., Wang, C., Yang, N., Ma, H., Ma, J., Russell, A.G., He, H., 2020. Air pollutant correlations in China: secondary air pollutant responses to NO_X and SO_2 control. Environ. Sci. Technol. Lett. 7 (10), 695–700. https://doi.org/10.1021/acs.estlett.0c00403.

Dong, Y., Li, J., Guo, J., Jiang, Z., Chu, Y., Chang, L., Yang, Y., Liao, H., 2020. The impact of synoptic patterns on summertime ozone pollution in the North China Plain. Sci. Total Environ. 735, 139559 https://doi.org/10.1016/j.scitotenv.2020.139559.

Gao, W., Tie, X., Xu, J., Huang, R., Mao, X., Zhou, G., Chang, L., 2017. Long-term trend of O_3 in a mega City (Shanghai), China: characteristics, causes, and interactions with precursors. Sci. Total Environ. 603–604, 425–433. https://doi.org/10.1016/j.scitotenv.2017.06.099.

Gong, C., Liao, H., 2019. A typical weather pattern for ozone pollution events in North China. Atmos. Chem. Phys. 19 (22), 13725–13740. https://doi.org/10.5194/acp-19-13725-2019.

He, C., Lu, X., Wang, H., Wang, H., Li, Y., He, G., He, Y., Wang, Y., Zhang, Y., Liu, Y., Fan, Q., Fan, S., 2022. The unexpected high frequency of nocturnal surface ozone enhancement events over China: characteristics and mechanisms. Atmos. Chem. Phys. 22 (23), 15243–15261. https://doi.org/10.5194/acp-22-15243-2022.

Hu, X.-M., Klein, P.M., Xue, M., Zhang, F., Doughty, D.C., Forkel, R., Joseph, E., Fuentes, J.D., 2013. Impact of the vertical mixing induced by low-level jets on boundary layer ozone concentration. Atmos. Environ. 70, 123–130. https://doi.org/10.1016/j.atmosenv.2012.12.046.

Jacob, D., 2000. Heterogeneous chemistry and tropospheric ozone. Atmos. Environ. 34 (12–14), 2131–2159. https://doi.org/10.1016/S1352-2310(99)00462-8.

Jena, C., Ghude, S.D., Beig, G., Chate, D.M., Kumar, R., Pfister, G.G., Lal, D.M., Surendran, D.E., Fadnavis, S., Van Der A, R.J., 2015. Inter-comparison of different NO_X emission inventories and associated variation in simulated surface ozone in Indian region. Atmos. Environ. 117, 61–73. https://doi.org/10.1016/j.atmosenv.2015.06.057.

Jia, S., Xu, X., Lin, W., Wang, Y., He, X., Zhang, H., 2015. Increased mixing ratio of surface ozone by nighttime convection process over the North China Plain. J. Appl. Meteorol. Sci. 26, 280–290. https://doi.org/10.11898/1001-7313.20150303.

Kulkarni, P.S., Bortoli, D., Silva, A.M., 2013. Nocturnal surface ozone enhancement and trend over urban and suburban sites in Portugal. Atmos. Environ. 71, 251–259. https://doi.org/10.1016/j.atmosenv.2013.01.051.

Lefohn, A.S., Malley, C.S., Smith, L., Wells, B., Hazucha, M., Simon, H., Naik, V., Mills, G., Schultz, M.G., Paoletti, E., De Marco, A., Xu, X., Zhang, L., Wang, T., Neufeld, H.S., Musselman, R.C., Tarasick, D., Brauer, M., Feng, Z., et al., 2018. Tropospheric ozone assessment report: Global ozone metrics for climate change, human health, and crop/ecosystem research. Elementa: Sci. Anthropocene 6, 27. https://doi.org/10.1525/elementa.279.

Li, K., Jacob, D.J., Liao, H., Qiu, Y., Shen, L., Zhai, S., Bates, K.H., Sulprizio, M.P., Song, S., Lu, X., Zhang, Q., Zheng, B., Zhang, Y., Zhang, J., Lee, H.C., Kuk, S.K., 2021. Ozone pollution in the North China Plain spreading into the late-winter haze season. Proc. Natl. Acad. Sci. USA 118 (10), e2015797118. https://doi.org/10.1073/pnas.2015797118.

Liao, Z., Pan, Y., Ma, P., Jia, X., Cheng, Z., Wang, Q., Dou, Y., Zhao, X., Zhang, J., Quan, J., 2023. Meteorological and chemical controls on surface ozone diurnal variability in Beijing: A clustering-based perspective. Atmos. Environ. 295, 119566 https://doi.org/10.1016/j.atmosenv.2022.119566.

Liu, Y., Wang, T., 2020. Worsening urban ozone pollution in China from 2013 to 2017 – Part 1: the complex and varying roles of meteorology. Atmos. Chem. Phys. 20 (11), 6305–6321. https://doi.org/10.5194/acp-20-6305-2020.

Ma, Z., Xu, J., Quan, W., Zhang, Z., Lin, W., Xu, X., 2016. Significant increase of surface ozone at a rural site, north of eastern China. Atmos. Chem. Phys. 16 (6), 3969–3977. https://doi.org/10.5194/acp-16-3969-2016.

Nuvolone, D., Petri, D., Voller, F., 2018. The effects of ozone on human health. Environ. Sci. Pollut. Control Ser. 25 (9), 8074–8088. https://doi.org/10.1007/s11356-017-9239-3.

Raff, J.D., Njegic, B., Chang, W.L., Gordon, M.S., Dabdub, D., Gerber, R.B., Finlayson-Pitts, B.J., 2009. Chlorine activation indoors and outdoors via surface-mediated reactions of nitrogen oxides with hydrogen chloride. Proc. Natl. Acad. Sci. USA 106 (33), 13647–13654. https://doi.org/10.1073/pnas.0904195106.

Ravishankara, A.R., 2009. Are chlorine atoms significant tropospheric free radicals? Proc. Natl. Acad. Sci. USA 106 (33), 13639–13640. https://doi.org/10.1073/pnas.0907089106.

Ren, Y., Zhang, H., Zhang, X., Wei, W., Li, Q., Wu, B., Cai, X., Song, Y., Kang, L., Zhu, T., 2021. Turbulence barrier effect during heavy haze pollution events. Sci. Total Environ. 753, 142286 https://doi.org/10.1016/j.scitotenv.2020.142286.

Salimi, F., Ristovski, Z., Mazaheri, M., Laiman, R., Crilley, L.R., He, C., Clifford, S., Morawska, L., 2014. Assessment and application of clustering techniques to atmospheric particle number size distribution for the purpose of source apportionment. Atmos. Chem. Phys. 14 (21), 11883–11892. https://doi.org/10.5194/acp-14-11883-2014.

San José, R., Stohl, A., Karatzas, K., Bohler, T., James, P., Pérez, J.L., 2005. A modelling study of an extraordinary night time ozone episode over Madrid domain. Environ. Model. Software 20 (5), 587–593. https://doi.org/10.1016/j.envsoft.2004.03.009.

Seinfeld, J.H., Pandis, S.N., 2016. Atmospheric Chemistry and Physics: from Air Pollution to Climate Change, third ed. John Wiley & Sons, Inc.

Su, T., Li, Z., Kahn, R., 2018. Relationships between the planetary boundary layer height and surface pollutants derived from lidar observations over China: regional pattern and influencing factors. Atmos. Chem. Phys. 18 (21), 15921–15935. https://doi.org/10.5194/acp-18-15921-2018.

Turner, M.C., Jerrett, M., Pope, C.A., Krewski, D., Gapstur, S.M., Diver, W.R., Beckerman, B.S., Marshall, J.D., Su, J., Crouse, D.L., Burnett, R.T., 2016. Long-term ozone exposure and mortality in a large prospective study. Am. J. Respir. Crit. Care Med. 193 (10), 1134–1142. https://doi.org/10.1164/rccm.201508-1633OC.

Wang, J., Wang, D., Ge, B., Lin, W., Ji, D., Pan, X., Li, J., Wang, Z., 2022a. Increase in daytime ozone exposure due to nighttime accumulation in a typical city in eastern China during 2014–2020. Atmos. Pollut. Res. 13 (4), 101387 https://doi.org/10.1016/j.apr.2022.101387.

Wang, X., Manning, W., Feng, Z., Zhu, Y., 2007. Ground-level ozone in China: distribution and effects on crop yields. Environ. Pollut. 147 (2), 394–400. https://doi.org/10.1016/j.envpol.2006.05.006.

Wang, X., Zhao, W., Zhang, T., Qiu, Y., Ma, P., Li, L., Wang, L., Wang, M., Zheng, D., Zhao, W., 2022b. Analysis of the characteristics of ozone pollution in the North China Plain from 2016 to 2020. Atmosphere 13 (5), 715. https://doi.org/10.3390/atmos13050715.

Wei, W., Fang, Y., Zhou, Y., 2021. Synoptic and meteorological drivers of regional ozone pollution events in China. Environ. Res. Commun. 3, 055004 https://doi.org/10.1088/2515-7620/abfe9c.

Yu, Y., Wang, Z., He, T., Meng, X., Xie, S., Yu, H., 2019. Driving factors of the significant increase in surface ozone in the Yangtze River Delta, China, during 2013–2017. Atmos. Pollut. Res. 10 (4), 1357–1364. https://doi.org/10.1016/j.apr.2019.03.010.

Yue, X., Unger, N., Harper, K., Xia, X., Liao, H., Zhu, T., Xiao, J., Feng, Z., Li, J., 2017. Ozone and haze pollution weakens net primary productivity in China. Atmos. Chem. Phys. 17 (9), 6073–6089. https://doi.org/10.5194/acp-17-6073-2017.

Zhang, R., Lei, W., Tie, X., Hess, P., 2004. Industrial emissions cause extreme urban ozone diurnal variability. Proc. Natl. Acad. Sci. USA 101 (17), 6346–6350. https://doi.org/10.1073/pnas.0401484101.

Zhang, Y., Ding, A., Mao, H., Nie, W., Zhou, D., Liu, L., Huang, X., Fu, C., 2016. Impact of synoptic weather patterns and inter-decadal climate variability on air quality in the North China Plain during 1980–2013. Atmos. Environ. 124, 119–128. https://doi.org/10.1016/j.atmosenv.2015.05.063.

Zong, L., Yang, Y., Gao, M., Wang, H., Wang, P., Zhang, H., Wang, L., Ning, G., Liu, C., Li, Y., Gao, Z., 2021. Large-scale synoptic drivers of co-occurring summertime ozone and $PM_{2.5}$ pollution in eastern China. Atmos. Chem. Phys. 21, 9105–9124. https://doi.org/10.5194/acp-21-9105-2021.